Geosci. Model Dev. Discuss., 7, 3647–3670, 2014
www.geosci-model-dev-discuss.net/7/3647/2014/
doi:10.5194/gmdd-7-3647-2014

Geoscientific Model Development Discussions
Open Access

Pan-spectral observing system simulation experiments of shortwave reflectance and longwave radiance for climate model evaluation

D. R. Feldman[1] **and W. D. Collins**[1,2]

[1]Lawrence Berkeley National Laboratory, Earth Sciences Division, 1 Cyclotron Road – MS 84R0171, Berkeley, CA 94720, USA
[2]University of California-Berkeley, Department of Earth and Planetary Science, Berkeley, USA

Received: 17 April 2014 – Accepted: 16 May 2014 – Published: 4 June 2014

Correspondence to: D. R. Feldman (drfeldman@lbl.gov)

Published by Copernicus Publications on behalf of the European Geosciences Union.

Abstract

Top-of-atmosphere spectrally-resolved shortwave reflectances and longwave radiances describe the evolution of the Earth's surface and atmosphere response to feedbacks in and human-induced forcings on the climate system. In order to evaluate proposed long-duration spectral measurements, we have projected 21st century changes described by the Community Climate System Model (CCSM3.0) conducted for the Intergovernmental Panel on Climate Change (IPCC) A2 Emissions Scenario onto shortwave reflectance spectra from 0.3 to 2.5 µm and longwave radiance spectra from 5 to 50 µm at 8 nm and 1 cm^{-1} resolution, respectively. The radiative transfer calculations have been rigorously validated against published standards and produce complementary signals describing the climate system forcings and feedbacks. Additional demonstration experiments were performed with the MIROC5 and HadGEM2-ES models for the Representative Concentration Pathway 8.5 (RCP8.5) scenario. The calculations contain readily distinguishable signatures of low clouds, snow/ice, aerosols, temperature gradients, and water vapour distributions. The goal of this effort is to understand both how climate change alters the spectrum of the Earth and determine whether spectral measurements enhance our detection and attribution of climate change. This effort also presents a path forward for hyperspectral measurement-model intercomparison by enabling a diverse set of comparisons between model results from coupled model intercomparisons and existing and proposed satellite instrument measurement systems.

1 Introduction

The spectrally-integrated upwelling top-of-atmosphere radiant energy field comprises the Earth system's total energy balance, and comprehensive comparisons of modelled Outgoing Longwave Radiation (OLR) and albedo with measurements of these quantities have led to important constraints on climate models (e.g., Morcrette, 1991; Kiehl et al., 1994). The spectrally resolved energy field spans an additional dimension that

GMDD
7, 3647–3670, 2014

contains information regarding the processes that govern that balance. Moreover, it has been demonstrated that infrared spectra contain important information that can be used to test climate models (e.g., Goody et al., 1998), primarily because the spectral signatures of individual forcings and feedbacks can be readily separated, detected, and quantified. Recent work by Roberts et al. (2011) suggest that shortwave spectra also contain independent information about processes that contribute to albedo, though the separability of processes that contribute to albedo from these spectra has not been addressed formally.

This has motivated the implementation of Observing System Simulation Experiments (OSSEs) based on climate models as a means for exploring the utility of well-posed comparisons between models and measurements. OSSEs have well-established techniques for evaluating the scientific and operational value of new instruments proposed for meteorological applications (Arnold and Dey, 1986). The role of OSSEs for climate science is less mature than that of the application to short-term forecasting for which they were originally developed. The long duration of climate studies and the necessarily long measurement records that are needed to confront models in their description of climate change motivate the development of climate model OSSEs. The forward evaluation of remote sensing signal sensitivity to uncertain model parametrisations and/or global climate sensitivity allows for an estimation of the value of certain types of remote sensing measurements where the underlying climate signal from the model is known. To that end, it has been recently noted by the Intergovernmental Panel on Climate Change (IPCC) that instrument simulators are valuable in that they can obviate inconsistencies between models and measurements (Flato et al., 2013).

Several investigations have explored direct comparisons between measurements from a variety of existing satellite-based instruments and simulations of those measurements based on various climate model integrations. For example, community-wide efforts have led to the establishment of the Cloud Feedback Model Intercomparison Project Observational Simulator Package (COSP) (Bodas-Salcedo et al., 2011), enabling inline instrument simulations for existing missions including the International

GMDD
7, 3647–3670, 2014

Satellite Cloud Climatology Project (ISCCP), the MODerate Resolution Imaging Spectroradiometer (MODIS), CloudSat, and Cloud-Aerosol Lidar and Infrared Pathfinder Satellite Observation (CALIPSO). Results from COSP based on models run in historical mode are then compared to existing measurement records to identify model biases (e.g., Kay et al., 2012; Pincus et al., 2012).

Additionally, there have been efforts to explore how hyperspectral measurements can be utilised for facile measurement-model intercomparison. Huang et al. (2007, 2010) and Leroy et al. (2008) examined longwave measurements and radio occultation simulations in detail and have compared the spectral signatures of variations in lapse rate, water vapour, and cloud radiative effects (CREs). The discrepancies in measured and modelled spectra suggest that the agreement in measured and modelled OLR is a result of compensating errors between temperature, water vapour, and cloud structure in the models.

Feldman et al. (2011a, b, 2013) have discussed how shortwave spectra may be considered for OSSEs. These works examined the utility of shortwave spectra for detecting climate change, and have found that shortwave measurements are more sensitive to low clouds and changes in frozen surface extent than are longwave spectral measurements.

Despite the potential utility of using visible, near-infrared, and infrared measurements, the simultaneous utilisation of shortwave reflectance and longwave radiance spectra to address climate change questions has not been explored in detail to date, despite the numerous studies based on coincident observations of broadband OLR and albedo (e.g., Kiehl and Trenberth, 1997; Hansen et al., 2005; Wielicki et al., 2006; Loeb et al., 2009). The combination of shortwave and longwave hyperspectral measurements could potentially be quite useful in addressing fundamental and unanswered questions related to shortwave cloud and ice feedbacks while simultaneously describing the temperature and water vapour structure of the atmosphere. The ultimate goal of this research area is to develop rigorous observational tests for climate models with a particular focus on using measurements to constrain climate model sensitivity.

GMDD
7, 3647–3670, 2014

Existing hyperspectral infrared measurement systems including the Atmospheric Infrared Sounder (AIRS) (Aumann et al., 2003) and the Infrared Atmospheric Sounding Interferometer (IASI) (Siméoni et al., 1997) can be considered as strong observational constraints. Moreover, hyperspectral shortwave measurements are available from the SCanning Imaging Absorption SpectroMeter for Atmospheric CHartographY (SCIAMACHY) (Bovensmann et al., 1999), and these extensive data records could be useful for measurement-model intercomparison.

This paper presents a versatile tool for simulating spectrally resolved measurements from the near-UV to the far-infrared and discusses how these measurements can be used to generalise existing OSSE efforts. The simulations are also designed for comprehensive science traceability studies for planned instruments such those recommended by the National Research Council's Decadal Survey including CLimate Absolute Radiance and Refractivity Observatory (CLARREO) (Wielicki et al., 2013) and GEOstationary Coastal and Air Pollution Events (GEO-CAPE) (Space Studies Board, 2007). Additionally, the pan-spectral OSSE may be utilised to develop climate model observational tests for evaluating results reported to the Coupled Model Intercomparison Project – Phase 5 (CMIP5) (Taylor et al., 2012) and Phase 6 (CMIP6) (Meehl et al., 2014).

2 Methodology

Following Feldman et al. (2011a), we present OSSE calculations of shortwave spectral reflectance and longwave spectral radiance that produce spectral measurements based on the climate projections conducted with Community Climate System Model, Version 3.0 (CCSM3) integrations (Collins et al., 2006a; Meehl et al., 2006). The spectral calculations are performed with the MODerate Resolution TRANsmission (MODTRAN™) radiative transfer code (Berk et al., 2005). The shortwave and longwave spectra are calculated from 0.3 to 2.5 µm (33 333 to 4000 cm^{-1}) at a 15 cm^{-1} native resolution (8 nm convolved instrument function), and from 5 to 50 µm (2000 to 200 cm^{-1})

GMDD
7, 3647–3670, 2014

at 1 cm^{-1} resolution, respectively. The calculations produce top-of-atmosphere (TOA) radiance spectra and upwelling and downwelling direct and diffuse spectral flux fields at each vertical level of CCSM3.

The fields produced in CCSM3 integrations include vertical profiles of atmospheric thermodynamic properties, trace gases, and condensed species on a 26 level hybrid-sigma grid extending from the surface to a constant pressure level of 2 hPa. CCSM3 has been run at a variety of different horizontal resolutions for the spectral-Eulerian atmospheric dynamical core. The results described here have been computed and archived at T85 resolution representing a triangular truncation of the dynamics at 85 wavenumbers and corresponding to a 1.4° equilateral grid on the equator. The OSSE, as described by Feldman et al. (2011a), utilises monthly-mean values for profiles of temperature, water vapour (H_2O), carbon dioxide (CO_2), ozone (O_3), methane (CH_4), nitrous oxide (N_2O), trichlorofluoromethane (CFC-11), and dichlorodifluoromethane (CFC12). Profiles of both liquid and ice cloud area, condensed water content, and effective radius are utilised. The treatment of cloud optics for the spectral simulations in the OSSE is identical to that used by the CCSM3. In the shortwave, the optical properties of liquid and ice clouds vary with wavelength (Feldman et al., 2011a). In the longwave, liquid and ice clouds are treated as grey bodies where liquid clouds are assigned a constant emissivity and ice clouds are assigned an emissivity that varies with the effective radii diagnosed for the constituent ice crystals (Ebert and Curry, 1992). The infrared absorption and scattering by aerosols are not included in the longwave OSSE, although the direct radiative effects are dust, sulfate, carbonaceous, and sea-salt aerosols are incorporated in the shortwave OSSE.

The treatment of the optical surface properties utilises the MODIS Bi-directional Reflectance Distribution Function (Schaaf et al., 2002) and has been critical for the realism of the shortwave OSSE (Feldman et al., 2011b) under present-day conditions. The formulation of the land-surface optical reflection reproduces the snow-free and snow-covered bidirectional reflectance properties from MODIS, and it also includes the effects of retreating snow cover on projections of the Earth's future reflectance field.

GMDD
7, 3647–3670, 2014

The longwave portion of the OSSE treats ocean surfaces with unitary emissivity, while land surface emissivity is based on an annually-cyclic monthly-mean climatology derived from spatial and temporal binning of the MODIS Land Surface Emissivity product (Wan and Zhao-Liang, 1997). By design, the effects of changes in sea-ice extent and snow cover are included in the OSSE calculations while the effects of future land-use and land-cover change and of changing soil moisture on near-infrared surface albedos are not.

This OSSE software framework requires multiple calls to the MODTRAN radiative transfer code and the OSSE is quite computationally expensive despite the optimised load-balancing and intrinsic parallelism of the calculations. Even though it is has been run on a massively parallel NASA High-End Computing facility, the ratio of OSSE computational time to the computational time to integrate the fully-coupled CCSM3 for the 21st century is approximately 50 : 1.

In support of the IPCC Fifth Assessment Report, modelling centres have undertaken significant efforts to produce a large set of model integrations for CMIP5. A similar infrastructure to the CCSM3 offline hyperspectral calculations was adopted for two climate models. These models were MIROC5 (Watanabe et al., 2010) and HadGEM2-ES (Jones et al., 2011), which lie on the low and high end of the model range of CMIP5 equilibrium climate sensitivities at 2.72 and 4.59 $^{\circ}$K/2 $\times$ CO_2, respectively (Andrews et al., 2012). Simulations were implemented for the first three decades of the Representative Concentration Pathway 8.5 (RCP8.5) scenario (Van Vuuren et al., 2011). The fields necessary to perform reflectance and radiance calculations in the OSSE have, unfortunately, only been archived at monthly-mean temporal resolution for this scenario. Due to the nonlinearity of radiative transfer, it is challenging to validate offline OSSE calculations with the reported values of albedo and OLR from these models, the latter of which are based on averages of radiation calculations performed with time-steps of a few minutes.

GMDD
7, 3647–3670, 2014

3 Results

In order to meet the requirement for high-accuracy calculations to support both mission design and climate model evaluation, there has been extensive validation performed on both the longwave and shortwave OSSE calculations based on CCSM3. As a result, the radiation calculations performed by MODTRAN are fully consistent with those produced by the CCSM3 radiation code, which itself is extensively evaluated against line-by-line models (Collins et al., 2006b; Oreopoulos et al., 2010). While the shortwave OSSE calculations from MODTRAN have already been extensively validated against CCSM3 all-sky and clear-sky albedo (Feldman et al., 2011a), the longwave fields are a new feature to the OSSE.

Longwave validation of the two codes was performed using a comparison of TOA OLR. Differences between the two radiative transfer schemes are less than 1 % for both clear- and all-sky conditions and arise from several factors. These factors include the contrasting treatments of clouds as vertically extended non-isothermal layers in MODTRAN vs. infinitely-thin isothermal objects in CCSM3 together with the contrasting solutions to the radiative equations using 8 discrete-ordinate streams in MODTRAN vs. two streams in CCSM3. Figure 1a and b shows a comparison between the OLR produced by the OSSE through offline calls to the CCSM3 longwave radiation code and the OLR produced from the MODTRAN instrument emulator. Figure 1b indicates the clear-sky calculations agree to better than $2\,\mathrm{W\,m^{-2}}$. Meanwhile, the level of agreement between the all-sky OLR from CCSM3 and MODTRAN is degraded relative to the clear-sky case, as shown in Fig. 1a, with a mean offset of $1\,\mathrm{W\,m^{-2}}$ and a root-mean-square (RMS) value of $3.1\,\mathrm{W\,m^{-2}}$. A closer investigation revealed that the differences in the numbers of streams in the radiative solution and level-layer formulation differences accounted for the all-sky discrepancies. This is consistent with the performance of the shortwave reflectance component of the OSSE, though the all-sky agreement between MODTRAN and the Community Atmosphere Model (CAM) component of CCSM3 exhibit less spread because the level-layer formulation discrepancy affects OLR more

GMDD
7, 3647–3670, 2014

than albedo. The agreement between MODTRAN and CAM for shortwave fluxes is shown in Fig. 1c and d with a mean offset of around 3 $W m^{-2}$ in all-sky conditions and 1 $W m^{-2}$ for clear-sky conditions, with good agreement at low solar zenith angles.

Globally-averaged longwave radiance and shortwave reflectance spectra are shown in Fig. 2a for both clear-sky and all-sky conditions at the beginning of the integration. This figure demonstrates many of the complementary features in these two spectral ranges, including the two window features in the visible and the mid-infrared which are affected by the presence of clouds, but clear-sky and all-sky differences are of opposite sign between the visible and infrared. Additionally, the spectra indicate a role of water vapour in reducing reflectance in the near-infrared overtone bands between 0.8 and 2.0 µm and producing rich spectral structure and decreased infrared radiance between 5 and 8.3 µm and 17 and 50 µm. Prominent greenhouse-gas absorption features are also indicated for CO_2, O_3, CH_4, and N_2O.

Figure 2b shows the corresponding globally-averaged trends in shortwave reflectances and longwave radiances during the first 50 years of the A2 scenario simulation. Several prominent features can be seen. First, the shortwave reflectances generally increase with the increased aerosol loading projected for the first half of the 21st century under both clear- and all-sky conditions. While much of the spatial and seasonal heterogeneity in shortwave reflectance trends that was identified in Feldman et al. (2011a) is averaged out in the globally and annually averaged trends, the contrast between clear-sky and all-sky reflectance trends gives an indication of the additional increase in reflectance from clouds. Also, the complex spectral structure in the wings of the near-infrared H_2O overtone bands indicates the shortwave forcing of greenhouse gases, a topic that deserves greater scrutiny (Collins et al., 2006b).

Meanwhile, longwave radiances show a decreasing trend around 6.3 µm due to greater atmospheric water vapour, increasing trends between 8 and 12 µm from higher surface skin temperatures, and decreasing trends between 14 and 16 µm from increased absorption in the wings of the mid-infrared CO_2 bands. The prescribed

GMDD
7, 3647–3670, 2014

increases in CH_4 and N_2O produce prominent signals around 7 µm, while increases in surface and tropospheric temperature are aliased into the H_2O mid- and far-IR bands.

Figure 3a–c shows differences in zonally-averaged shortwave reflectance and longwave radiance spectra for clear-sky and all-sky conditions and cloud radiative effect (CRE) between the decade from 2050–2059 and the first decade of the 21st century, while Fig. 3d–f shows the differences between 2090–2099 and the first decade of the 21st century. Increases in anthropogenic aerosol loading between the decades of the 2000s and the 2050s result in increased clear-sky reflectance at low latitudes and visible and near-infrared wavelengths during that time period. Concurrent changes in the frozen surface coverage decrease reflectance at higher latitudes in the window band but not in the near-infrared. Differences in all-sky reflectance share some similarities to differences in the clear-sky reflectance, but striping features covering in the water-vapour overtone bands are also present and are indicative of movement in low-level stratus clouds. Additionally, movement of the InterTropical Convergence Zone (ITCZ) produces a dipole in reflectance near the equator with diminished striping features across the overtone bands.

The changes in both all-sky and clear-sky longwave radiance exhibit the spectral features highlighted in Fig. 2b. The only other prominent feature is the polar amplification of surface temperature warming that produces meridional gradients in the window band. Changes in cloud cover over this period lead to decreases in the radiance across the spectrum except between 14 and 16 µm around the ITCZ. Additionally, the stratospheric cooling and increased CO_2 are prominent around 15 µm while increasing CH_4 and N_2O produce significant signals around 7 µm.

Differences in zonally- and annually-averaged shortwave reflectance and longwave radiance between the start and end of the 21st century under the A2 emissions scenario are shown in Fig. 3d–f. These spectra show decreased frozen surface extent at high latitudes in visible reflectances and increased water vapour loading leading to lower reflectances in the water vapour overtone bands and at 6.3 µm and in the far-infrared H_2O rotational band. All-sky pan-spectral simulations reveal the shifts in

GMDD
7, 3647–3670, 2014

storm-tracks with striping features in the H_2O near-infrared overtone bands at mid-latitudes, and they reveal a stronger dipole near the ITCZ near the equator across the shortwave and longwave.

OSSEs can also be used for inter-model comparisons. To demonstrate this, we considered the contributions of the MIROC5 and HadGEM2-ES models to the CMIP5 archive. Difference trends in albedo and OLR are shown in Fig. 4a–d. In all-sky OLR, trend differences indicate model disagreement in deep convective response in the Tropical Western Pacific, with HadGEM2-ES showing increased deep convection as compared to MIROC5, though the sign of trends is reversed over South America. The clear-sky OLR trend differences are small, but spatially expansive and are due in large part to the water vapour response both in convective and subsidence regions. The MIROC5 model exhibits a water vapour loading response that impacts OLR more than the HadGEM2-ES model.

For climate sensitivity, however, the difference in shortwave response of these models is larger. Differences in the models' description of sea-ice loss and cloud response at high latitudes and particularly in subsidence regions, have been shown to contribute most significantly to the discrepancy in their equilibrium sensitivities (Andrews et al., 2012). Hyperspectral simulations based on these models have been validated with a bias of $3\,W\,m^{-2}$ and an RMS difference of 0.5 and $3\,W\,m^{-2}$ for clear-sky and all-sky longwave, respectively, with respect to the model-reported TOA fluxes. For the shortwave simulations, the hyperspectral simulations exhibit a bias of 0.1 % and an RMS difference of 1.5 % and 2.2 % for clear-sky and all-sky, respectively, subject to the above-mentioned issues with temporal averaging. Nevertheless, Fig. 4e and f indicates that there are numerous differences in the models' response in hyperspectral simulations in subsets of the OSSE spectra from the Arctic and the Tropical Western Pacific (TWP). Both the visible and infrared window spectral regions readily differentiate the two climate model runs, and spectral trends of the model differ significantly. Also, in the TWP, the sign of the change in the shortwave visible differs from that of the near-infrared water vapour overtone regions, potentially improving signal detectability,

GMDD
7, 3647–3670, 2014

and indicating the potential for spectra to identify processes that contribute to different trends in OLR and albedo. The corollary of this is that long-term spectral trends from measurements can be confronted with the results of a hyperspectral simulator from model to exclude one or more model descriptions of the response to known forcings.

Hyperspectral instrument simulators such as the one presented here enable researchers to explore the spectral dimension of climate change to understand how various processes contribute to changes in albedo and OLR. The large number of data points generated by this pan-spectral OSSE provide numerous opportunities for measurement-model intercomparison, and the contrasting performance of the OSSE in the visible and infrared windows and near-infrared water vapour overtone bands and mid-infrared vibration-rotation bands provide an indication for the potential benefit for the construction of combined shortwave and longwave spectral fingerprints (e.g., Leroy and Anderson, 2010) of climate change.

4 Discussion

This paper has introduced a software framework that is capable of simulating the shortwave and longwave TOA spectral signatures of the climate change diagnosed from projections based on global climate and Earth system models. The pan-spectral simulations span from the near-UV to the far-infrared and indicate a rich level of information content. Long-term measurements of changes in these quantities will capture many of the climate change processes and the relationships between these processes that are sources of uncertainty in climate models. They also indicate that the shortwave measurements are much more spatially heterogeneous than the longwave measurements, so analysis of globally-averaged changes in shortwave spectra is less suited towards diagnosing the processes that contribute to spectral changes than detailed examination of spatially resolved differences.

The ultimate goal of this research is to understand both how climate change alters the evolution of the Earth's spectrum and determine whether spectral measurements

GMDD
7, 3647–3670, 2014

enhance our detection and attribution of climate change. The pan-spectral OSSE described here will enable formal comparisons between models and a broad suite of planned and existing instrumentation, and will help establish observational metrics for differentiating between climate models according to specific processes. This may also enhance the current efforts to utilise the highly-regularised climate model reporting framework of the CMIP5 to simulate specific instrumentation through the Observational Simulator Package (COSP) (Bodas-Salcedo et al., 2011). As of this writing, the COSP framework (version 1.3.1) currently has an ISCCP, MODIS, CloudSat, and CALIPSO instrument emulators. It can be linked with the Radiative Transfer for Television Infrared Observation Satellite Operational Vertical Sounder (RTTOV) (Saunders et al., 1999), which is a hyperspectral mid-infrared simulator, but that package has only been developed for clear-sky applications. Regardless, is a critical need to develop the methodology to utilise the spectral dimension to gauge model performance. Recent works by Roberts et al. (2011, 2013) provide a path forward for how this can be undertaken quantitatively using principal components, and these tools may be helpful for the modelling community for narrowing the range in reported shortwave feedback.

A primary challenge to the utilisation of instrument simulators for model and measurement-model intercomparison is their large computational expense. For pan-spectral simulators, the expense is even more significant, with over 70 % arising from the shortwave simulation. However, it should be noted that we found a contrast between the visible and near-infrared response to climate change, with the former largely controlled by spectrally-flat features and the latter controlled by the interaction between clouds, aerosols, water vapour, and greenhouse gases. Spectral resolution is required to capture those interactions in the near-infrared. Moreover, Roberts et al. (2011) showed that the principal component spectrum from SCIAMACHY measurements changed significantly between 25 and 100 nm Full-Width Half Max (FWHM) resolution, suggesting that information about shortwave processes requires dozens of channels, but not thousands. The computational expense can be lowered with ultra-fast radiative transfer methods (e.g., Liu et al., 2006). Alternatively, regional calculations may be

GMDD
7, 3647–3670, 2014

considered for addressing those regions that contribute most significantly to climate sensitivity divergence (Armour et al., 2013). Finally, while the computational expense of the calculations presented here is extreme, this approach does have the potential to encompass a large number of existing and proposed measurement concepts. It is much more of a challenge to use narrow-band simulators to explore the value of new mission concepts.

For competent simulation, it is critical that model intercomparison projects, such as those of CMIP5, archive the fields necessary to perform offline diagnostic radiative transfer across the electromagnetic spectrum. This includes the three-dimensional thermodynamic, gaseous, and condensate structure of the atmosphere, and land emission and reflectance at time-scales sub-daily time-scales. The Cloud Feedback Model Intercomparison Project (Bony et al., 2011) archived these fields for snapshots of several experiments associated with CMIP5, but the level of participation by the modelling centres was less than for the CMIP5 Tier 1 experiments including RCP8.5.

Spectra can be a very important tool for measurement model intercomparison, but OSSE development needs to be expanded to consider existing hyperspectral data records, which contain numerous indicators of processes that control the Earth's energy balance. As of the writing of this paper, the data record from AIRS is over 11 years long, the IASI record is over 7 years long, and the SCIAMACHY record is over 10 years long. These decadal length records provide an opportunity to test present day climate model performance in multiple ways that cannot be easily be adjusted with problematic tuning (Mauritsen et al., 2012) and can therefore be strict constraints for model development and testing. However, the challenges that have faced other long-term satellite data record analyses (Norris, 2007; Clement et al., 2009; Spencer and Christy, 1992; Fu and Johanson, 2004; Seidel et al., 2011) must be considered. While orbit and calibration are considerably less problematic for newer instrumentation, the climate quality of the instantaneous retrievals must be established. This pan-spectral simulation capability may also be applicable to recent efforts by CLARREO and GEO-CAPE to develop the pan-spectral instrumentation in order to answer questions related to the processes

GMDD
7, 3647–3670, 2014

that contribute to TOA atmospheric energetics and also the evolution of tropospheric chemistry.

The community should consider how the advent of pan-spectral measurements may have the potential to detect climate change and to distinguish which climate models produce more realistic projections, sooner than is possible with conventional broadband instruments (Feldman et al., 2013). Spectral Empirical Orthogonal Functions may accelerate this ability to distinguish models even further by exploiting spectral redundancy to minimise noise and discern spectral multi-pole features less readily detected with broadband instruments. Pan-spectral techniques can then be used to detect low-cloud feedbacks sooner and with greater accuracy than broadband or spectral infrared techniques alone. Optimal detection techniques (e.g., Newchurch et al., 2003; Leroy and Anderson, 2010) are critical to establishing how the hyperspectral dimension can be utilised to detect climate change and assess models.

Acknowledgements. Funding for this research was supported by NASA grants NNX10AK27G, and NNX11AE65G and NASA High-End Computing grants SMD-08-0999, SMD-09-1397, and SMD-10-1799. This work was also supported by Contractor Supporting Research (CSR) funding from Berkeley Lab, provided by the Director, Office of Science, of the US Department of Energy under Contract No. DE-AC02-05CH11231. The following individuals also contributed: David Young, Bruce Wielicki, and Rosemary Baize of the NASA Langley Research Center, Tsengdar Lee of the NASA Science Mission Directorate, and Lex Berk of Spectral Sciences, Inc.

References

Andrews, T., Gregory, J. M., Webb, M. J., and Taylor, K. E.: Forcing, feedbacks and climate sensitivity in CMIP5 coupled atmosphere-ocean climate models, Geophys. Res. Lett., 39, L09712, doi:10.1029/2012GL051607, 2012.

Armour, K. C., Bitz, C. M., and Roe, G. H.: Time-varying climate sensitivity from regional feedbacks, J. Climate, 26, 4518–4534, doi:10.1175/JCLI-D-12-00544.1, 2013.

GMDD

7, 3647–3670, 2014

Arnold Jr., C. P. and Dey, C. H.: Observing-systems simulation experiments: past, present, and future, B. Am. Meteorol. Soc., 67, 687–695, 1986.

Aumann, H. H., Chahine, M. T., Gautier, C., Goldberg, M. D., Kalnay, E., McMillin, L. M., Revercomb, H., Rosenkranz, P., Smith, W., Staelin, D., Strow, L., and Susskind, J.: AIRS/AMSU/HSB on the Aqua mission: design, science objectives, data products, and processing systems, IEEE T. Geosci. Remote, 41, 253–264, 2003.

Berk, A., Anderson, G. P., Acharya, P. K., Bernstein, L. S., Muratov, L., Lee, J., and Lewis, P. E.: MODTRAN 5: a reformulated atmospheric band model with auxiliary species and practical multiple scattering options: update, in: Defense and Security, International Society for Optics and Photonics, 662–667, 2005.

Bodas-Salcedo, A., Webb, M. J., Bony, S., Chepfer, H., Dufresne, J.-L., Klein, S. A., Zhang, Y., Marchand, R., Pincus, R., and John, V. O.: COSP: satellite simulation software for model assessment, B. Am. Meteorol. Soc., 92, 1023–1043, 2011.

Bony, S., Webb, M., Bretherton, C., Klein, S. A., Siebesma, P., Tselioudis, G., and Zhang, M.: CFMIP: towards a better evaluation and understanding of clouds and cloud feedbacks in CMIP5 models, Clivar Exchanges, 56, 20–22, 2011.

Bovensmann, H., Burrows, J. P., Buchwitz, M., Frerick, J., Noël, S., Rozanov, V. V., Chance, K. V., and Goede, A. P. H.: SCIAMACHY: mission objectives and measurement modes, J. Atmos. Sci., 56, 127–150, 1999.

Clement, A. C., Burgman, R., and Norris, J. R.: Observational and model evidence for positive low-level cloud feedback, Science, 325, 460–464, 2009.

Collins, W. D., Bitz, C. M., Blackmon, M. L., Bonan, G. B., Bretherton, C. S., Carton, J. A., Chang, P., Doney, S. C., Hack, J. J., Henderson, T. B., Kiehl, J. T., Large, W. G., McKenna, D. S., Santer, B. D., and Smith, R. D.: The Community Climate System Model: CCSM3, J. Climate, 19, 2122–2143, 2006a.

Collins, W. D., Ramaswamy, V., Schwarzkopf, M. D., Sun, Y., Portmann, R. W., Fu, Q., Casassanova, S. E. B., Dufresne, J.-L., Fillmore, D. W., Forster, P. M. D., Galin, V. Y., Gohar, L. K., Ingram, W. J., Kratz, D. P., Lefebvre, M.-P., Li, J., Marquet, P., Oinas, V., Tsushima, Y., Uchiyama, T., and Zhong, W. Y.: Radiative forcing by well-mixed greenhouse gases: estimates from climate models in the Intergovernmental Panel on Climate Change (IPCC) Fourth Assessment Report (AR4), J. Geophys. Res.-Atmos. (1984–2012), 111, D14317, doi:10.1029/2005JD006713, 2006b.

GMDD
7, 3647–3670, 2014

Ebert, E. E. and Curry, J. A.: A parameterization of ice cloud optical properties for climate models, J. Geophys. Res., 97, 3831–3836, 1992.
Feldman, D. R., Algieri, C. A., Ong, J. R., and Collins, W. D.: CLARREO shortwave observing system simulation experiments of the twenty-first century: simulator design and implementation, J. Geophys. Res.-Atmos., 116, D10107, doi:10.1029/2010JD015350, 2011a.
Feldman, D. R., Algieri, C. A., Collins, W. D., Roberts, Y. L., and Pilewskie, P. A.: Simulation studies for the detection of changes in broadband albedo and shortwave nadir reflectance spectra under a climate change scenario, J. Geophys. Res.-Atmos., 116, D24103, doi:10.1029/2011JD016407, 2011b.
Feldman, D. R., Coleman, D. M., and Collins, W. D.: On the usage of spectral and broadband satellite instrument measurements to differentiate climate models with different low-cloud feedback strengths, J. Climate, 26, I 6561–6574, doi:10.1175/JCLI-D-12-00378.1, 2013.
Flato, G., Marotzke, J., Abiodun, B., Braconnot, P., Chou, S. C., Collins, W., Cox, P., Driouech, F., Emori, S., Eyring, V., Forest, C., Gleckler, P., Guilyardi, E., Jakob, C., Kattsov, V., Reason , C., and Rummukainen, M.: Evaluation of Climate Models, in: Climate Change 2013: The Physical Science Basis. Contribution of Working Group I to the Fifth Assessment Report of the Intergovernmental Panel on Climate Change, edited by: Stocker, T. F., Qin, D., Plattner, G.-K., Tignor, M., Allen, S. K., Boschung, J., Nauels, A., Xia, Y., Bex, V., and Midgley, P. M., Cambridge University Press, Cambridge, UK and New York, NY, USA, 2013.
Fu, Q. and Johanson, C. M.: Stratospheric influences on MSU-derived tropospheric temperature trends: a direct error analysis, J. Climate, 17, 4636–4640, 2004.
Goody, R., Anderson, J., and North, G.: Testing climate models: an approach, B. Am. Meteorol. Soc., 79, 2541–2549, 1998.
Hansen, J., Nazarenko, L., Ruedy, R., Sato, M., Willis, J., Del Genio, A., Kock, D., Lacis, A., Lo, K., Menon, S., Novakov, T., Perlwitz, J., Russell, G., Schmidt, G., and Tausnev, N.: Earth's energy imbalance: confirmation and implications, Science, 208, 1431–1435, 2005.
Huang, Y., Ramaswamy, V., Huang, X., Fu, Q., and Bardeen, C.: A strict test in climate modeling with spectrally resolved radiances: GCM simulation versus AIRS observations, Geophys. Res. Lett., 34, L24707, doi:10.1029/2007GL031409, 2007.
Huang, Y., Leroy, S. S., and Anderson, J. G.: Determining longwave forcing and feedback using infrared spectra and GNSS radio occultation, J. Climate, 23, 6027–6035, 2010.
Jones, C. D., Hughes, J. K., Bellouin, N., Hardiman, S. C., Jones, G. S., Knight, J., Liddicoat, S., O'Connor, F. M., Andres, R. J., Bell, C., Boo, K.-O., Bozzo, A., Butchart, N.,

GMDD
7, 3647–3670, 2014

Cadule, P., Corbin, K. D., Doutriaux-Boucher, M., Friedlingstein, P., Gornall, J., Gray, L., Halloran, P. R., Hurtt, G., Ingram, W. J., Lamarque, J.-F., Law, R. M., Meinshausen, M., Osprey, S., Palin, E. J., Parsons Chini, L., Raddatz, T., Sanderson, M. G., Sellar, A. A., Schurer, A., Valdes, P., Wood, N., Woodward, S., Yoshioka, M., and Zerroukat, M.: The HadGEM2-ES implementation of CMIP5 centennial simulations, Geosci. Model Dev., 4, 543–570, doi:10.5194/gmd-4-543-2011, 2011.

Kay, J. E., Hillman, B. R., Klein, S. A., Zhang, Y., Medeiros, B., Pincus, R., Gettelman, A., Eaton, B., Boyle, J., Marchand, R., and Ackerman, T. P.: Exposing global cloud biases in the Community Atmosphere Model (CAM) using satellite observations and their corresponding instrument simulators, J. Climate, 25, 5190–5207, 2012.

Kiehl, J. T. and Trenberth, K. E.: Earth's annual global mean energy budget, B. Am. Meteorol. Soc., 78, 197–208, 1997.

Kiehl, J. T., Hack, J. J., and Briegleb, B. P.: The simulated Earth radiation budget of the National Center for Atmospheric Research community climate model CCM2 and comparisons with the Earth Radiation Budget Experiment (ERBE), J. Geophys. Res., 99, 20815–20827, doi:10.1029/94JD00941, 1994.

Leroy, S., Anderson, J., Dykema, J., and Goody, R.: Testing climate models using thermal infrared spectra, J. Climate, 21, 1863–1875, 2008.

Liu, X., Smith, W. L., Zhou, D. K., and Larar, A.: Principal component-based radiative transfer model for hyperspectral sensors: theoretical concept, Appl. Optics, 45, 201–209, 2006.

Loeb, N. G., Wielicki, B. A., Doelling, D. R., Smith, G. L., Keyes, D. F., Kato, S., Manalo-Smith, N., and Wong, T.: Toward optimal closure of the Earth's top-of-atmosphere radiation budget, J. Climate, 22, 748–766, 2009.

Mauritsen, T., Stevens, B., Roeckner, E., Crueger, T., Esch, M., Giorgetta, M., Haak, H., Jungclaus, J., Klocke, D., Matei, D., Mikolajewicz, U., Notz, D., Pincus, R., Schmidt, H., and Tomassini, L.: Tuning the climate of a global model, Journal of Advances in Modeling Earth Systems, 4, M00A01, doi:10.1029/2012MS000154, 2012.

Meehl, G. A., Washington, W. M., Santer, B. D., Collins, W. D., Arblaster, J. M., Hu, A., Lawrence, D. M., Teng, H., Buja, L. E., and Strand, W. G.: Climate change projections for the twenty-first century and climate change commitment in the CCSM3, J. Climate, 19, 2597–2616, 2006.

Meehl, G. A., Moss, R., Taylor, K. E., Eyring, V., Stouffer, R. J., Bony, S., and Stevens, B.: Climate model intercomparison: preparing for the next phase, EOS T. Am. Geophys. Un., 95, p. 77, 2014.

GMDD
7, 3647–3670, 2014

Morcrette, J.-J.: Radiation and cloud radiative properties in the European Centre for Medium Range Weather Forecasts Forecasting system, J. Geophys. Res., 96, 9121–9132, doi:10.1029/89JD01597, 1991.

Nakicenovic, N., Davidson, O., Davis, G., Grübler, A., Kram, T., Lebre La Rovere, E., Metz, B., Morita, T., Pepper, W., Pitcher, H., Sankovski, A., Shukla, P., Swart, R., Watson, R., and Dadi, Z.: Special Report on Emissions Scenarios: a Special Report of Working Group III of the Intergovernmental Panel on Climate Change, Cambridge University Press, Cambridge, UK, 599 pp., 2000.

Norris, J. R.: Observed interdecadal changes in cloudiness: real or spurious?, in: Climate Variability and Extremes During the Past 100 Years, Springer Netherlands, 169–178, 2007.

Oreopoulos, L. and Mlawer, E.: MODELING: the Continual Intercomparison of Radiation Codes (CIRC) assessing anew the quality of GCM radiation algorithms, B. Am. Meteorol. Soc., 91, 305–310, 2010.

Pincus, R., Platnick, S., Ackerman, S. A., Hemler, R. S., and Patrick Hofmann, R. J.: Reconciling simulated and observed views of clouds: MODIS, ISCCP, and the limits of instrument simulators, J. Climate, 25, 4699–4720, 2012.

Roberts, Y. L., Pilewskie, P., and Kindel, B. C.: Evaluating the observed variability in hyperspectral Earth-reflected solar radiance, J. Geophys. Res.-Atmos., 116, D24119, doi:10.1029/2011JD016448, 2011.

Roberts, Y. L., Pilewskie, P., Kindel, B. C., Feldman, D. R., and Collins, W. D.: Quantitative comparison of the variability in observed and simulated shortwave reflectance, Atmos. Chem. Phys., 13, 3133–3147, doi:10.5194/acp-13-3133-2013, 2013.

Saunders, R., Matricardi, M., and Brunel, P.: An improved fast radiative transfer model for assimilation of satellite radiance observations, Q. J. Roy. Meteor. Soc., 125, 1407–1425, 1999.

Schaaf, C. B., Gao, F., Strahler, A. H., Lucht, W., Li, X., Tsang, T., Strugnell, N. C., Zhang, X., Jin, Y., Muller, J.-P., Lewis, P., Barnesly, M., Hobson, P., Disney, M., Roberts, G., Dunderdale, M., Doll, C., d'Entremont, R. P., Hu, B., Liang, S., Privette, J. L., and Roy, D.: First operational BRDF, albedo nadir reflectance products from MODIS, Remote Sens. Environ., 83, 135–148, 2002.

Seidel, D. J., Gillett, N. P., Lanzante, J. R., Shine, K. P., and Thorne, P. W.: Stratospheric temperature trends: our evolving understanding, Climate Change, 2, 592–616, 2011.

Siméoni, D., Singer, C., and Chalon, G.: Infrared atmospheric sounding interferometer, Acta Astronaut., 40, 113–118, 1997.

GMDD
7, 3647–3670, 2014

Space Studies Board: Earth Science and Applications from Space: National Imperatives for the Next Decade and Beyond, National Academies Press, Washington DC, 456 pp., 2007.
Spencer, R. W. and Christy, J. R.: Precision and radiosonde validation of satellite gridpoint temperature anomalies. Part II: A tropospheric retrieval and trends during 1979–90, J. Climate, 5, 858–866, 1992.
Taylor, K. E., Stouffer, R. J., and Meehl, G. A.: An overview of CMIP5 and the experiment design, B. Am. Meteorol. Soc., 93, 485–498, 2012.
Van Vuuren, D. P., Edmonds, J., Kainuma, M., Riahi, K., Thomson, A., Hibbard, K., Hurtt, G., Kram, T., Krey, V., Lamarque, J.-F., Masui, T., Meinshausen, M., Nakicenovic, N., Smith, S., and Rose, S. K.: The representative concentration pathways: an overview, Climatic Change, 109, 5–31, 2011.
Wan, Z. and Zhao-Liang, L.: A physics-based algorithm for retrieving land-surface emissivity and temperature from EOS/MODIS data, IEEE T. Geosci. Remote, 35, 980–996, 1997.
Watanabe, M., Suzuki, T., O'ishi, R., Komuro, Y., Watanabe, S., Emori, S., Takemura, T., Chikira, M., Ogura, T., Sekiguchi, M., Takata, K., Yamazaki, D., Yokohata, T., Nozawa, T., Hasumi, H., Tatebe, H., and Kimoto, M.: Improved climate simulation by MIROC5: mean states, variability, and climate sensitivity, J. Climate, 23, 6312–6335, 2010.
Wielicki, B. A., Charlock, T. P., Doelling, D. R., Kratz, D. P., Loeb, N. G., Minnis, P., Priestley, K. J., and Young, D. F.: CERES radiation budget accuracy overview, Preprints, 12th Conf. Atmospheric Radiation, Madison, WI, Amer. Meteor. Soc., 9.1, 2006.
Wielicki, B. A., Young, D. F., Mlynczak, M. G., Thome, K. J., Leroy, S., Corliss, J., Anderson, J. G., Ao, C., Bantges, R., Best, F., Bowman, K., Brindley, H., Butler, J. J., Collins, W., Dykema, J. A., Doelling, D. R., Feldman, D. R., Fox. N., Huang, X., and Holz, R.: Achieving climate change absolute accuracy in orbit, B. Am. Meteorol. Soc., 94, 1519–1539, doi:10.1175/BAMS-D-12-00149.1, 2013.

GMDD
7, 3647–3670, 2014

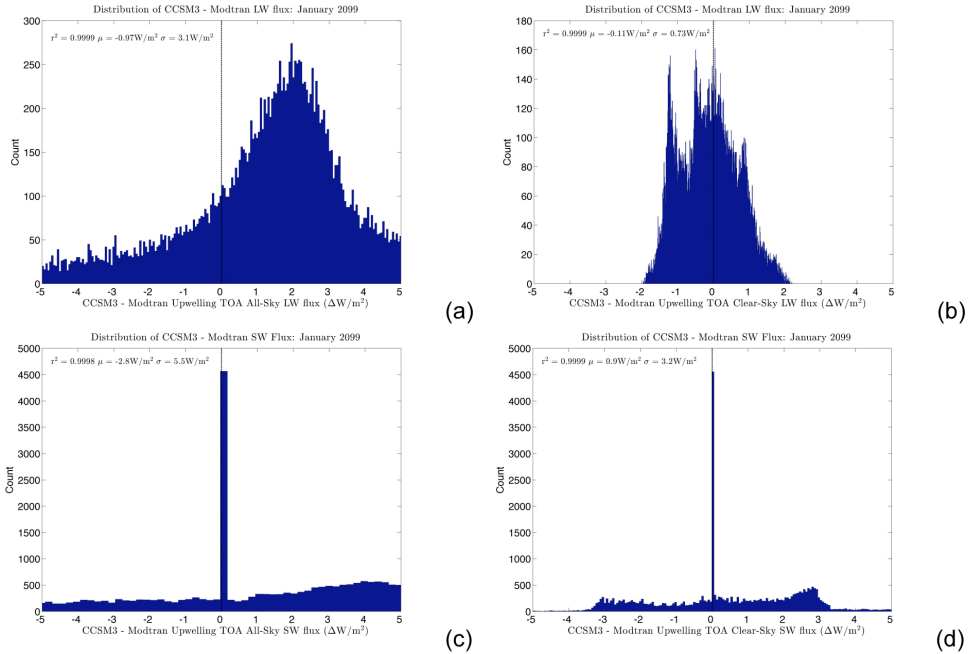

Figure 1. (a) Scatterplot of all grid points for the all-sky OLR calculated by the CCSM radiative transfer code and by MODTRAN for the 32 768 grid boxes from January 2000 for the A2 simulation. Also included are the Pearson correlation coefficient (r^2) and the mean (μ) and standard deviation (σ) of the differences between the two codes. **(b)** Same as **(a)** but for clear-sky OLR. **(c)** Same as **(a)** but for all-sky shortwave flux. **(d)** Same as **(b)** but for clear-sky shortwave flux.

GMDD
7, 3647–3670, 2014

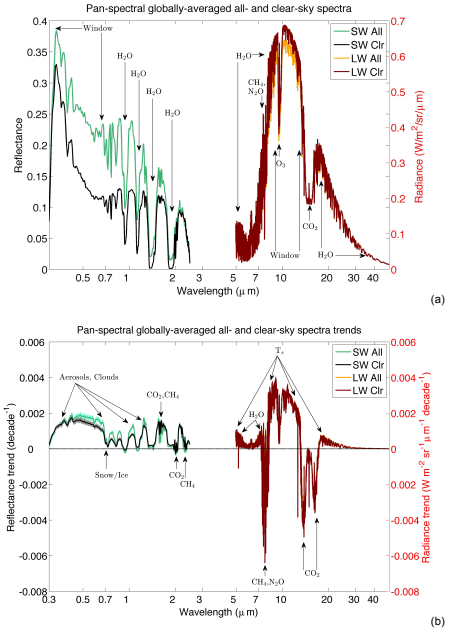

Figure 2. (a) Pan-spectral composite of the globally-averaged all- and clear-sky shortwave reflectance and longwave radiance from January 2000 for the A2 simulation. **(b)** Same as **(a)** but showing the trends in shortwave reflectance (in reflectance units) and longwave radiance (in W m^{-2} sr^{-1} μm^{-1}). Shading indicates 95 % confidence interval of uncertainty in trends.

GMDD
7, 3647–3670, 2014

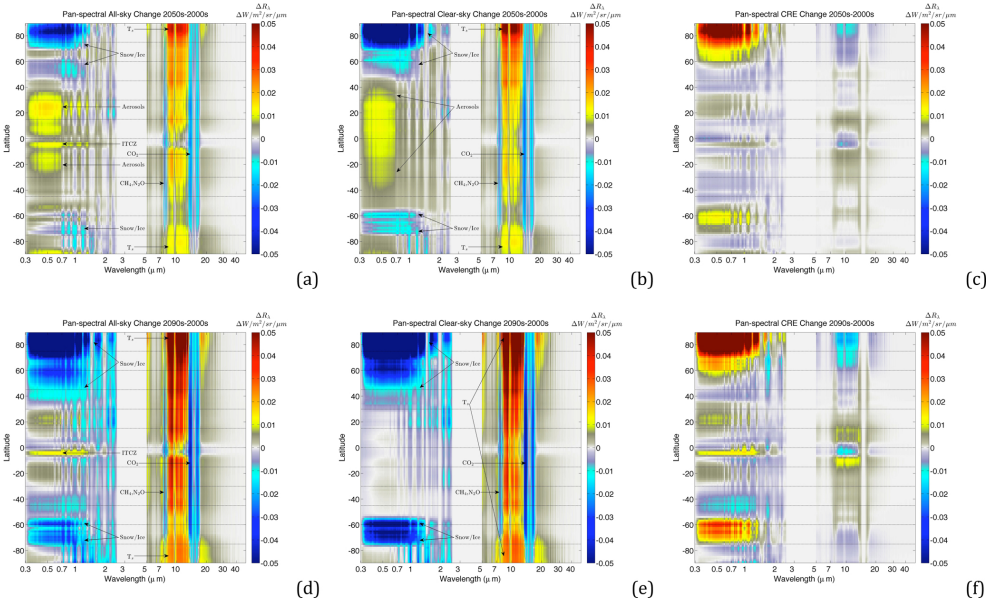

Figure 3. (a) Differences in zonally- and decadally-averaged pan-spectral clear-sky composite for 2050–2059 and 2000–2009 for the A2 simulation. **(b)** Same as **(a)** but plotting differences in all-sky conditions between the 2050s and the 2000s. **(c)** Differences in cloud radiative effect (CRE) between the 2050s and 2000s. **(d)** Same as **(a)** but plotting differences between the 2090s and the 2000s. **(e)** Same as **(d)** but plotting all-sky conditions. **(f)** Same as **(c)** but plotting differences between the 2090s and 2000s.

GMDD
7, 3647–3670, 2014

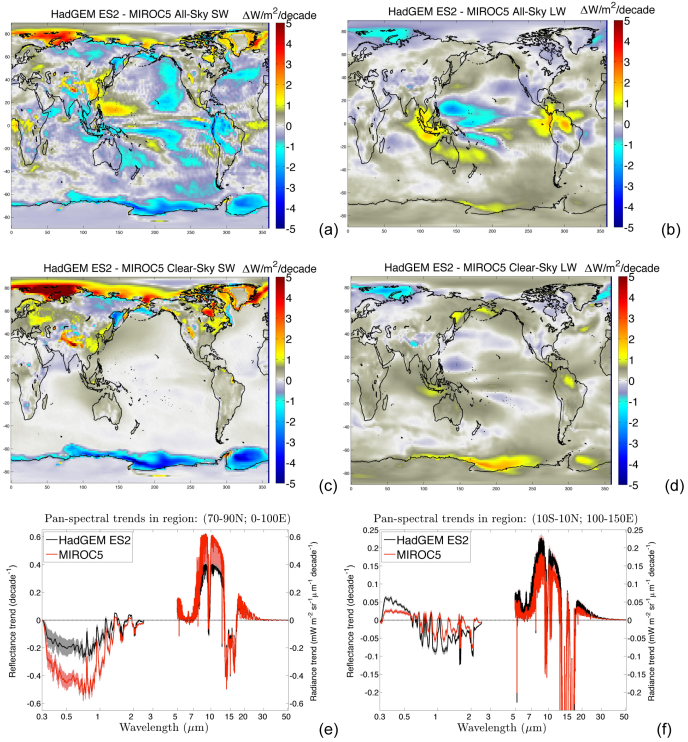

Figure 4. (a) Difference in all-sky shortwave TOA flux trends between HadGEM2-ES and MIROC5 running the RCP8.5 scenario over the period 2005–2035. **(b)** Same as **(a)** but for longwave TOA flux trends. **(c)** Same as **(a)** but for clear-sky shortwave TOA flux trends. **(d)** Same as **(a)** but for clear-sky longwave TOA flux trends. **(e)** Pan-Spectral all-sky trends shortwave reflectance and longwave radiance for the MIROC5 and HadGEM2-ES models derived for the Arctic (70–90° N; 0–100° E) and **(f)** for the Tropical Western Pacific (10° S–10° N; 100–150° E).

GMDD
7, 3647–3670, 2014